entropy

MDPI

Article

# Experimental Study of Single Phase Flow in a Closed-Loop Cooling System with Integrated Mini-Channel Heat Sink

**Lei Ma [1,2], Xuxin Zhao [2], Hongyuan Sun [2], Qixing Wu [2] and Wei Liu [3,*]**

[1] Key Laboratory of Optoelectronic Devices and Systems of Ministry of Education and Guangdong Province, Shenzhen University, Shenzhen 518060, China; leima@szu.edu.cn

[2] Key Laboratory of New Lithium-ion Batteries and Mesoporous Materials of Shenzhen City, College of Chemistry and Environmental Engineering, Shenzhen University, Shenzhen 518060, China; zhaoxx@szu.edu.cn (X.Z.); hysun163@163.com (H.S.); qxwu@szu.edu.cn (Q.W.)

[3] School of Energy and Power Engineering, Huazhong University of Science and Technology, Wuhan 430074, China

* Correspondence: w_liu@hust.edu.cn; Tel.: +86-27-8754-2618; Fax: +86-27-8754-0724

Academic Editor: Milivoje M. Kostic

Received: 16 November 2015; Accepted: 1 April 2016; Published: 2 June 2016

**Abstract:** The flow and heat transfer characteristics of a closed-loop cooling system with a mini-channel heat sink for thermal management of electronics is studied experimentally. The heat sink is designed with corrugated fins to improve its heat dissipation capability. The experiments are performed using variable coolant volumetric flow rates and input heating powers. The experimental results show a high and reliable thermal performance using the heat sink with corrugated fins. The heat transfer capability is improved up to 30 W/cm$^2$ when the base temperature is kept at a stable and acceptable level. Besides the heat transfer capability enhancement, the capability of the system to transfer heat for a long distance is also studied and a fast thermal response time to reach steady state is observed once the input heating power or the volume flow rate are varied. Under different input heat source powers and volumetric flow rates, our results suggest potential applications of the designed mini-channel heat sink in cooling microelectronics.

**Keywords:** thermal management; mini-channel heat sink; corrugated fins; single phase flow

## 1. Introduction

With ever increasing integration density in microelectronic chips, thermal management has become a main challenge in the design of integrated circuits [1–5]. Though the high electronic integration requires more power supply and therefore poses a big challenge for thermal management, the temperature of each device is constrained by the reliability limits to obtain a satisfactory system performance for electronic equipment due to the fact that the devices show degraded performance or can even be damaged if the generated heat cannot be dissipated effectively. To increase heat dissipation in microelectronics, the traditional solution is to increase the available heat transfer area, for example, by the use of different kinds of fins in heat exchangers. This solution, however, requires a larger heat exchange system and shows a limited enhancement in cooling devices with high heat flux and thus is undesirable. An alternate solution is to use mini- and micro-channels that can provide an effective way of cooling small surfaces through convection.

The first mini- or micro-channel heat sink described by Tuckerman and Pease [6] in 1981 could dissipate heat flux up to 790 W/cm$^2$ when the substrate temperature was below 71 °C. Following their pioneering work, different kinds of mini or micro-channel heat sink have been extensively investigated [7–17]. Vafai *et al.* [7] proposed a two-layer heat sink with counter flow

arrangement and their result showed that such design substantially improved the cooling performance over conventional one-layer micro-channel heat sinks. Peng *et al.* [9] experimentally analyzed the effect of heat sink structural parameters on the flow and heat transfer characteristics. Kandlikar *et al.* [10] presented several complex heat sink structures with fabrication technology and observed some performance enhancement. Steinke *et al.* [11] reviewed several heat transfer enhancement techniques for single-phase flow in mini- and micro-channels such as the flow transition, boundary layer breakup, entrance region, vibration, electric fields, swirl flow, secondary flow and mixers. For the liquid flow friction factor in heat sink, Steinke *et al.* [12] suggested that entrance/exit pressure loss be considered when results were compared with the conventional theory. Liu *et al.* [15] developed a longitudinal vortex generator (LVG) in a rectangular channel heat sink and found that laminar-to-turbulent transition occurred at Reynolds numbers of 600–720. Bower *et al.* [16] designed a SiC heat sink and showed favorable overall heat transfer coefficient for a single row SiC heat exchanger compared with a validation heat exchanger fabricated from copper. However, the heat transfer coefficient in multiple row heat sinks did not agree well with the laminar flow theory. Using both experimental and numerical approaches, Qu and Mudawar [18,19] investigated the heat transfer and pressure drop in the heat sink. Their results indicated that the conventional Navier–Stokes and energy equations could adequately predict the heat transfer and flow characteristics in micro-channel heat sink. Morini [20] intensively reviewed the single phase convective heat transfer in micro-channels and analyzed some main results, such as friction factor, laminar-to-turbulent transition, and the Nusselt number.

Among the vast majority of applications of micro-channel heat sink, NASA designed a micro-channel heat exchanger that was used in the model X-38 re-entry vehicle and could dissipate 3.1 kW heat energy when the inlet mixture of ethylene glycol and water was at 4.4 °C [21]. JPL manufactured a silicon heat sink which could remove up to 25 W/cm$^2$ heat flux when the volume flow rate was 20 mL/min [22]. Stanford [23] made a heat exchanger which could remove 25 W/cm$^2$ heat flux when the volume flow rate was 70 mL/min and the exchanger temperature remained below 80 °C. Bintoro *et al.* [24] presented a closed-loop electronics cooling system by implementing single phase impinging jet and mini-channels heat exchanger and their system could remove 200 W heat when the chip temperature was below 95 °C and the ambient temperature was about 30 °C.

As described before, most previous work mainly focused on the investigation of heat transfer and flow characteristics of mini- or micro-channel. Generally, a larger heat flux can be achieved with smaller area of heat source surface. However, the micro-channel leads to high pressure drop and power consumption if it is applied in cooling the macro-scale heat source. Mini-channel can adequately work in such a condition with a moderate volume flow rate and pressure drop. An open-loop cooling system is often used as the experimental apparatus in the study of micro- or mini-channel performance. However, few study was reported on closed-loop cooling system. In this work, we design a compact and integrated cooling system with a novel mini-channel heat sink that comes with corrugated. We focus not only on the flow and heat transfer characteristics of the heat sink, but also on the stability and the performance of the whole cooling system, such as the transportation distance, response time, and system pressure drop.

## 2. Experimental Apparatus

### 2.1. Experimental System

The flow diagram of our closed-loop cooling system is shown in Figure 1. The system comprises of four main components, including the heat sink, the radiator, the reservoir, and the pump. As the key component, the heat sink is characterized for closed-loop with distilled water as working fluid to remove the heat from a heat source. The working fluid is pumped into the heat sink to reject the heat generated by the heat source. The heated working fluid is cooled in the radiator along the flow direction and then returns to the reservoir to continue the next cycle driven by a gear pump through a rotameter flow meter that measures the volumetric flow rate.

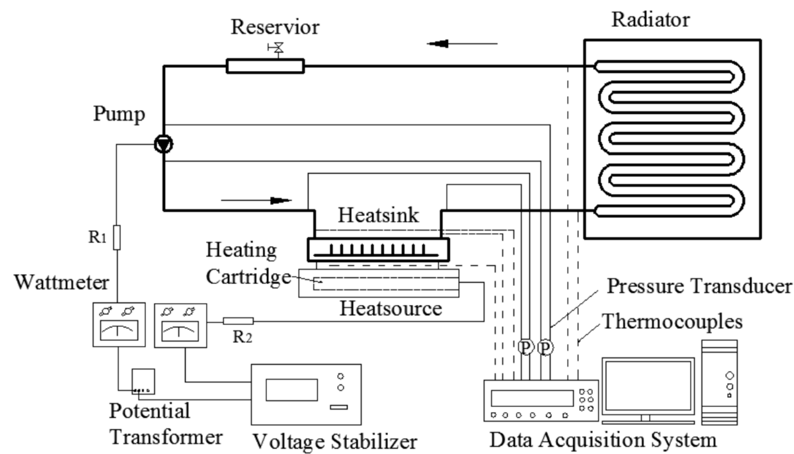


**Figure 1.** Schematic of the experimental system.

The mini-channel heat sink with corrugated fins and the radiator plate are made of brass and aluminum, respectively. The reservoir and the transportation pipes are made of stainless steel. The radiator is the heat rejecter to remove the heat to the environment. Some bubbles may appear after the cooling system operates for a long time. The bubbles, if existing, are blocked in the reservoir. The originally contained air in the system is discharged to reach a vacuum condition before the working fluid is filled in the reservoir.

### 2.2. Design of the Mini-Channel Heat Sink

The design of the mini-channel heat sink aims at removing the heat generated from the heat source with a moderate flow rate to ensure a reasonable pressure drop and power consumption of the entire loop. The mini-channel heat sink consists of some corrugated fins based on the notion that the heat transfer performance of heat sink can be enhanced due to much more turbulence generated by the fins. Considering that the maldistribution effect of working fluid in the heat sink may lead to serious non-uniform temperature profile [25], two inlets/outlets are designed in our system. The heat sink is integrated with three components: top plate with fins, bottom plate with fins, and outer frame. Two plates are designed separately with staggered fins arrangement, because of the difficulty in manufacturing a corrugated channel in a single plate. Welding is utilized to combine these three parts, as well as to connect the heat sink and system pipes.

Figure 2 shows the schematic of the heat sink. The outer frame's dimension is 46 mm ($L$) $\times$ 26 mm ($W$). The thickness of the frame is 2 mm. All the fins on the plate have the same dimension, of which length $L_w$ is 5 mm and width $W_w$ is 0.5 mm. The height of fins and fluid channel is 1.5 mm, and the parallel spacing between fins $W_c$ is 1.5 mm. The fins are designed by a staggered arrangement, *i.e.*, 27 fins are designed at the top plate and the staggered 24 fins are designed at the bottom plate. The angle $\alpha$ between the fin and outer frame side is 27.65°. The inlet and outlet pipes pattern are 3 mm $\times$ 0.5 mm circular tube, and the main system's transportation pipes pattern is 6 mm $\times$ 1 mm circular tube. In order to make the heat sink and the heat source compact, a substrate attached to the heat sink with a dimension of 40 mm $\times$ 20 mm $\times$ 0.5 mm is designed as the interface with the heat source.

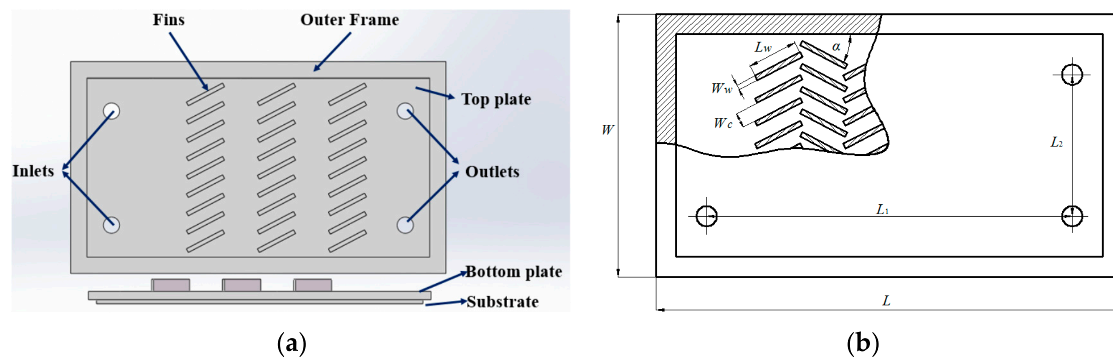


**Figure 2.** Schematic of heat sink. (**a**) Separate component schematic; (**b**) Compact schematic of heat sink.

## 2.3. Design of Radiator

We originally focus on the cooling system adaptable to the space environment. Due to the limitation of experimental condition, the fin-tube radiator is designed to be utilized on land to simulate the environment in space with additional cooling pipes integrated. As shown in Figure 3, the main plate is manufactured with a single aluminum plate, which has a dimension of 1092 mm × 552 mm × 2 mm. Since the design of our radiator follows reference [26], the details will not be discussed here. The front view shows that the main system pipes are parallel arranged to make the radiator more compact and light. The unit of the radiator is shown in Figure 3b. The heat from the main system pipes can be conducted to the other side of the main plate effectively and is finally removed by the cooling water with a cooling system that is not shown here.

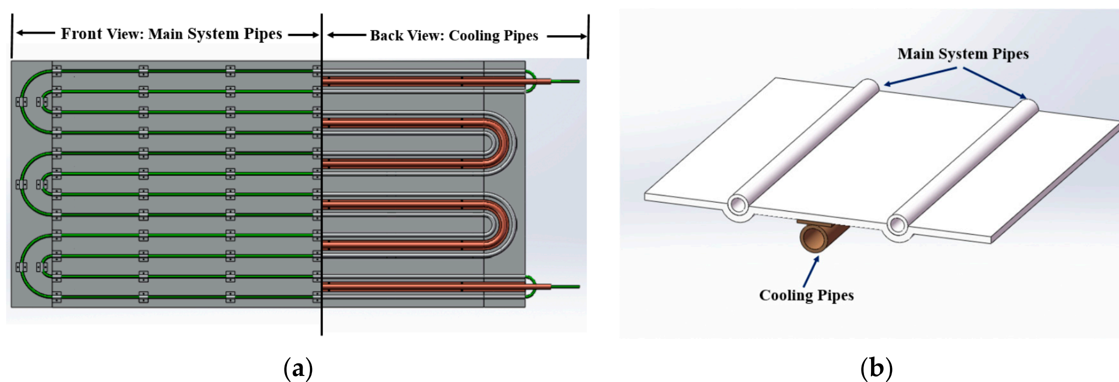


**Figure 3.** Schematic of radiator. (**a**) Schematic of the overall radiator; (**b**) Schematic of one unit cell of the radiator.

## 2.4. Design of the Heat Source

As shown in Figure 4, the heat source provides the power up to 320 W with a uniform heat flux at the interface, which has a dimension of 40 mm × 20 mm. Two holes with diameter of 6.5 mm are drilled into the bottom part of the heat source to locate two cartridge heaters (each of 160 W). Measured and adjusted by a wattmeter, the cartridge heaters are connected in parallel and powered by a 0–220 V AC power supply. As illustrated in Figure 5, the heat sink and the heat source are tightly pressed with epoxy resin plate. Thermal grease (~1 $Wm^{-1} \cdot K^{-1}$) is used to reduce the thermal resistance between the heat sink and the heat source.

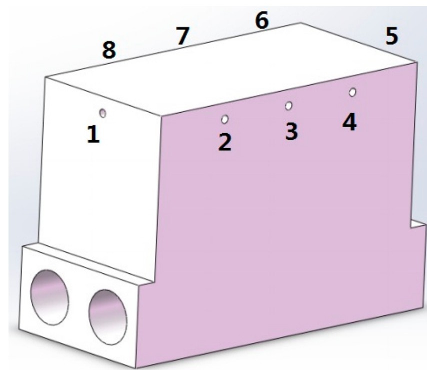


**Figure 4.** Schematic of the heat source (1~8: thermocouples locations).

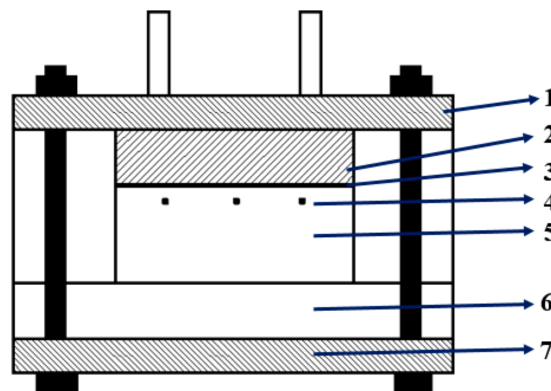


**Figure 5.** The compact of heat sink (1-the epoxy resin plate, 2-mini-channel heat sink, 3-thermal grease, 4-thermocouples, 5-heat source, 6-insulation plate, 7-bottom epoxy resin plate).

*2.5. Temperature and Pressure Testing*

The entire heat sink is hermetically sealed with insulation material to minimize the heat loss to the ambient. The pump in the system that forces the coolant to pass through the heat sink is adjusted by a wattmeter. Additional testing transducers are added to measure the temperatures and pressures at the inlet/outlet of the heat sink during the test.

As shown in Figure 4, below the top surface of heat source are eight micro holes with a diameter of 1 mm that are drilled into the side wall of the heat sink. Eight thermocouples are inserted into these holes to measure the temperature distribution at the surface of the heat source. At the inlet/outlet of the heat sink, thermocouples are stuck to the outer of the stainless pipes to measure the inlet/outlet fluid temperature. Other thermocouples are located at the inlet and outlet of the radiator and in the air to measure the radiator inlet, outlet and room temperature, respectively. Shown as dashed lines in Figure 1, all the thermocouples with calibration in the system are T-type.

In Figure 6, a stainless conjunction is designed to converge/allocate the flow at inlet/outlet of the heat sink. A micro-hole is drilled at the other side of the conjunction and pressure transducer is connected to measure the pressure drop between the inlet and exit of the heat sink. The pressure drop between in inlet and outlet of heat sink as well as the inlet and outlet of pump are obtained, respectively, to analyze the flow characteristics of the heat sink and the whole cooling system. As mentioned before and shown in Figure 6, the two inlets and outlets pipes pattern is 3 mm $\times$ 0.5 mm circular tubes, and the main system transportation pipes pattern is 6 mm $\times$ 1 mm circular tube.

All the temperature and pressure data are collected and sent to the PC system and automatically recorded through a data acquisition system. Experiments are conducted with various volume flow rates ranging from 100 to 400 mL/min.

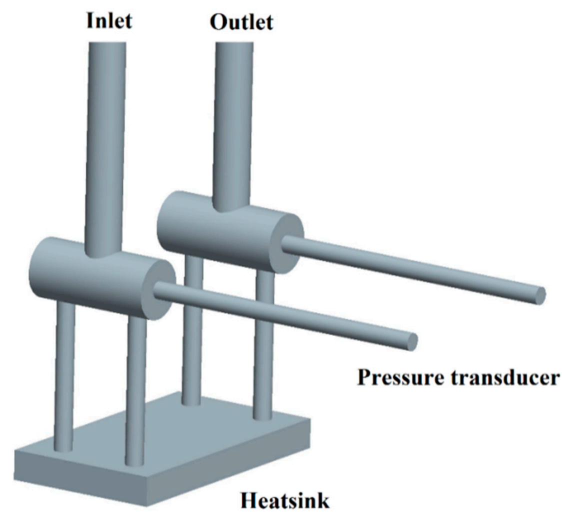


**Figure 6.** Schematic of the inlet/outlet conjunction.

### 2.6. Data Reduction

The heat transfer coefficient (HTC) of the heat sink is expressed as follows:

$$h = \frac{q}{T_w - T_l} \tag{1}$$

where $q$ is the heat flux at the substrate surface generated by the heat source; $T_w$ and $T_l$ are the average temperature of the base of heat sink and the liquid, respectively, expressed as follows:

$$T_w = \frac{\sum_{i=1}^{n} T_i}{n}, n = 8 \tag{2}$$

$$T_l = \frac{T_{s,in} + T_{s,out}}{2} \tag{3}$$

where $T_i$ is the temperature of thermal couple inserted to measure the temperature distribution at the surface of heat source as shown in Figure 4; $T_{s,in}$ and $T_{s,out}$ represent the inlet and outlet liquid temperature of the heat sink, respectively.

### 2.7. Uncertainty in Experimental Data

The test range and accuracy of measurements are given in Table 1. The uncertainties of the experimental data are calculated following Reference [27]. It involves calculating variable derivatives with respect to each experimental parameter and applies the already-known uncertainties that are calculated as follows:

$$U_R = \sqrt{\sum_{i=1}^{n} \left( \frac{\partial R}{\partial x_i} U_{xi} \right)^2} \tag{4}$$

where $R = f\ (x_1, x_2, \ldots, x_n)$ represents a desired variable; $x_1, x_2, \ldots, x_n$ are the variables that influence $R$, and their absolute uncertainties are expressed by $U_{x1}, U_{x2}, \ldots, U_{xn}$, respectively. After calculation, the uncertainties for temperature, pressure drop and the heat transfer coefficient are 0.62%–2.34%, 0.24%–4.10%, and 1.41%–8.22%, respectively, when the volume flow rate ranges from 100 to 400 mL/min as shown in Table 2.

**Table 1.** Test range and accuracy of instruments.

| Instruments | Range | Accuracy |
|---|---|---|
| T-type thermocouples | −40 to 100 °C | 0.5 °C |
| Pressure drop transducer for heat sink | 7500 Pa | 25 Pa |
| Pressure drop transducer for total system | 130,000 Pa | 100 Pa |

**Table 2.** Experiment uncertainties.

| Objects | Uncertainty |
|---|---|
| Temperature | ± (0.62%–2.34%) |
| Pressure drop | ± (0.24%–4.10%) |
| Heat transfer coefficient | ± (1.41%–8.22%) |

## 3. Results and Discussions

### *3.1. Heat Sink Performance*

During the test, the inlet volume flow rate varies from 100 mL/min to 400 mL/min with a sequential 50 mL/min augmentation. The heat source power varies from 0 to 240 W with an increase of 20 W each step. Figure 7 illustrates the temperature response with different inlet volume flow rate and heat source power. Liquid temperature reaches the peak at the exit of the heat sink. The fluid absorbs much more heat and the liquid temperature at the outlet of the heat sink increases with more heat source power input. The heated liquid water is cooled in the radiator and its temperature decreases to room temperature level. Finally, the cooled water is forced to pass through the heat sink to continue the next cycle.

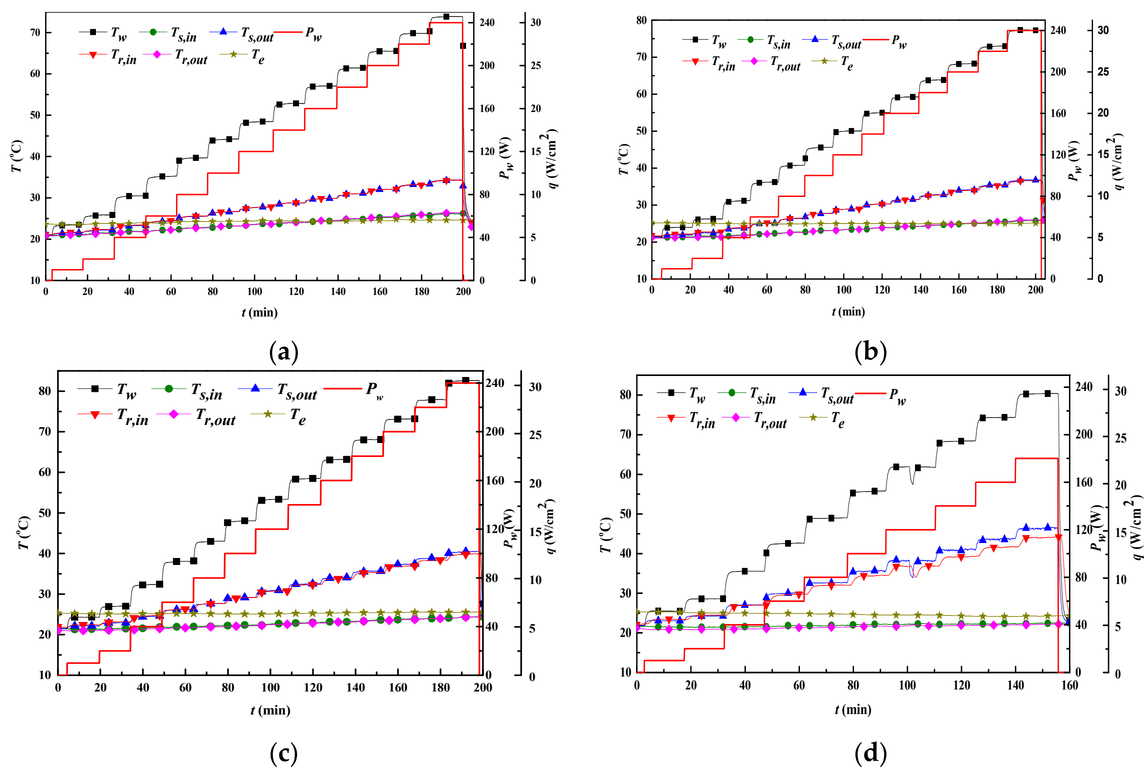


**Figure 7.** Temperature response with different volume flow rate. (**a**) 400 mL/min; (**b**) 300 mL/min; (**c**) 200 mL/min; (**d**) 100 mL/min.

The main objective of the cooling system is to minimize the base temperature as well as the heat source temperature and to remain at a stable and acceptable level. The distribution of the base temperature is consistent and the average temperature is 74 °C when the heat source power is 240 W and volume flow rate is 400 mL/min. When the base temperature is 77.3 °C and the heat source power is 240 W (corresponding to a heat flux of 30 W/cm$^2$), the volume flow rate can be controlled as low as 300 mL/min. As the room temperature almost remains around 23 °C, the liquid temperature at the exit of the radiator remains at the same level, and the temperature difference between inlet and outlet of the heat sink decreases with increasing inlet volume flow rate.

Figure 8 shows the heat transfer coefficient (HTC) and pressure drop in heat sink as a function of volume flow rate. With the increase of volume flow rate, the convection heat transfer is improved and thus the overall HTC increases rapidly. When the input heating power is 180 W, the HTC of heat sink is 4554.98 W/m$^2$· K at a volume flow rate of 100 mL/min, and the HTC is 6361.80 W/m$^2$· K when the volume flow rate reaches 400 mL/min. Obviously the pressure drop increases as the volume flow rate increases as shown in Figure 8b. Meanwhile, the slope of the pressure drop also increases with an increase in volume flow rate. Two reasons may explain the change of the slope in the pressure drop characteristics. One is that the increase of volume flow rate lowers the average liquid temperature and thus increases water intrinsic viscosity, resulting in a larger pressure drop. This effect can be proved with the result that the pressure drop increases with the augmentation of input heating power when the volume flow rate is at 350 mL/min and 400 mL/min. The other is that inlet and outlet pressure losses are proportional to the velocity squared [18], therefore increasing volume flow rate can lead to a more pronounced increase in pressure penalty. When the heat source power is 240 W and volume flow rate is 400 mL/min, the pressure drop is 6473.95 Pa.

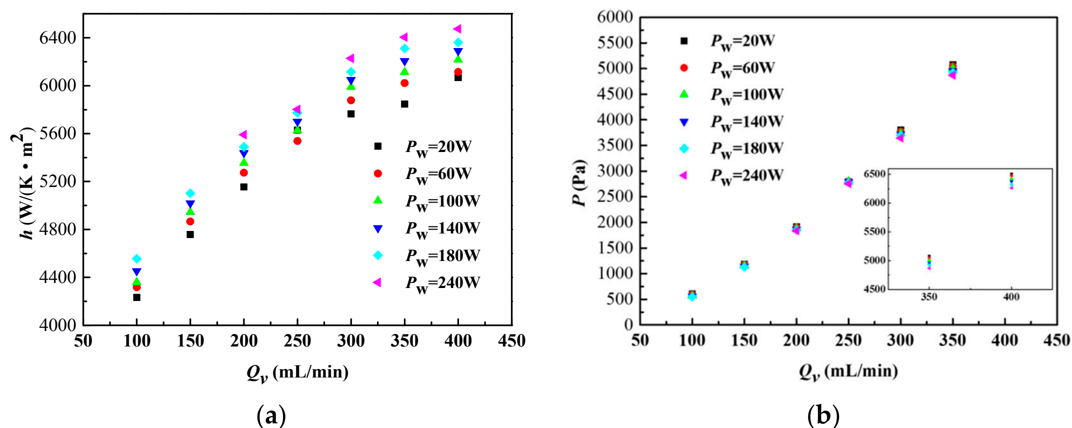


**Figure 8.** Heat sink performance. (**a**) HTC as the function of volume flow rate; (**b**) pressure drop as the function of volume flow rate.

The performance of the heat sink in the cooling system is compared with [28] and [29] on HTC and temperature response with different heat source power. The calculation of Reynolds numbers is based on the properties of distilled water under 40 °C. As shown in Figure 9, HTC ($P_w$ equal to 240 W) is around 1.5 times than literature data even with loaded nano-particle. The average base temperature (volume flow rate equal to 400 mL/min) is also much lower than literature data under variable heat flux, as shown in Figure 10.

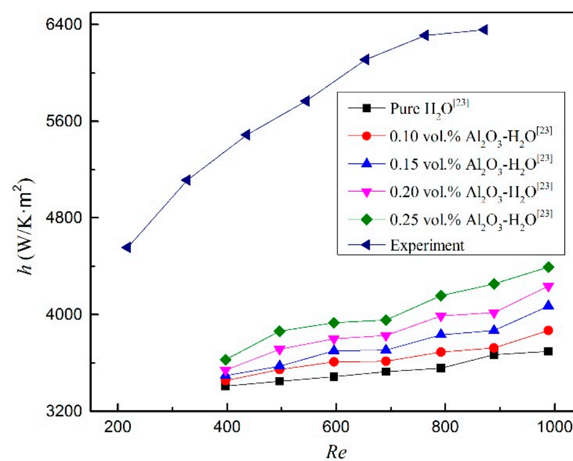


**Figure 9.** Comparison on HTC as the function of *Re*.

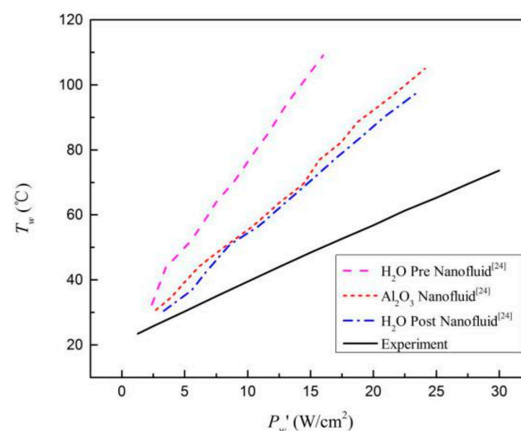


**Figure 10.** Comparison on base temperature as the function of unit heat source power.

### *3.2. The Closed-Loop System Performance*

As the heat source, such as electronic devices, may be located far away from the heat rejecter, such as a radiator, the heat transportation capability with a long distance must be considered. The system performance and stability must be analyzed. The presented closed-loop system aims to remove the heat of the heat source in a long transportation distance of more than 5 m and the whole system pipe length is more than 11 m, excluding the system pipes in the radiator. The overall mass of this closed-loop integrated mini-channel heat sink cooling system is less than 10 kg, including the heat sink, radiator, reservoir, pump, and system pipes.

Figure 11 illustrates the temperature response when the heat source power increases from 80 W to 100 W at the volume flow rate of 100 mL/min. We can see that the liquid temperature at the exit of heat sink and inlet of the radiator almost remains the same order of magnitude, with similar behavior observed at the exit of radiator and inlet of the heat sink. Therefore, it indicates, to some extent, that the heat loss from the system pipes to the ambient is negligible and heat transfer mainly occurs at the radiator and heat sink. It can be clearly seen that the base temperature and outlet temperature of the heat sink increase prior to the temperature rise of the radiator inlet liquid. This process is mainly affected by the relative position of these components in the system and heat transfer in such a long distance system should have a finite response time. The whole system reaches a steady state in 2 min after the input heating power is changed. Therefore, this closed-loop cooling system has a swift response to the input heating power variation, and it can be operated well under steady state operation without temperature fluctuation.

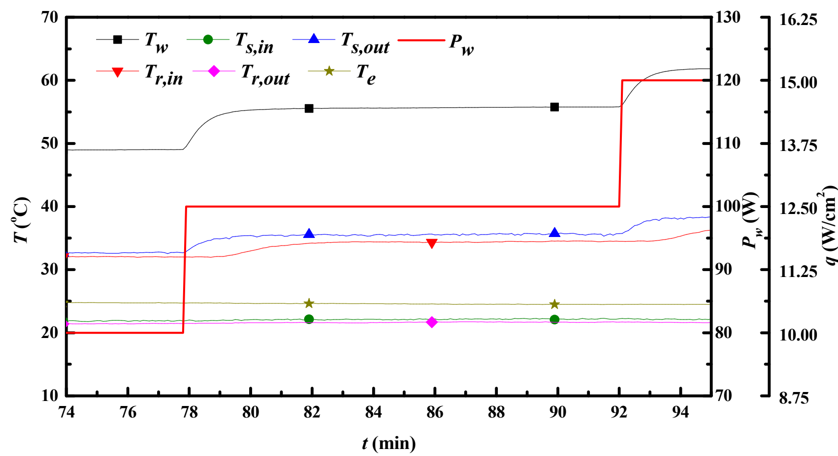


**Figure 11.** System response (flow rate = 100 mL/min, heat source power = 100 W).

When the heat source power is fixed at 160 W (corresponding to a heat flux of 20 W/cm$^2$), the temperature response under different volume flow rates is shown in Figure 12. It indicates that the cooling system can be operated well and the base temperature stays below 75 °C when the heat source power is less than 160 W. Figure 13 illustrates the whole system pressure drop when the heat source power is 160 W and this response is similar to the pressure drop between the inlet and outlet of the heat sink. The pressure drop increases extraordinarily with increasing volume flow rate. When the system flow rate is 100 and 400 mL/min, the system pressure drop is 6.24 and 41.31 kPa, respectively.

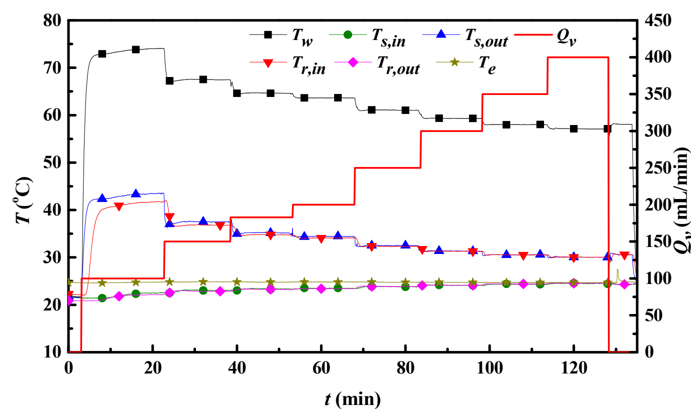


**Figure 12.** Temperature response at 20 W/cm$^2$.

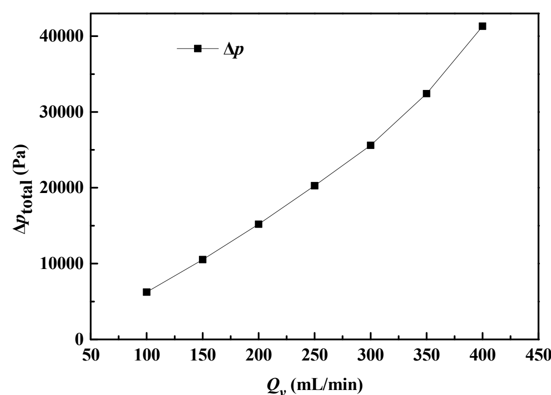


**Figure 13.** System pressure drop as a function of volume flow rate.

## 4. Conclusions

This work presents an experimental study of single phase flow and heat transfer characteristics in a compact closed-loop cooling system with integrated mini-channel heat sink. The whole cooling system shows a stable and reliable performance with approximately 2 min response time to achieve steady state once the input heating power or system volume flow rate are changed. The main conclusions are as follows:

(a) The system has a transportation distance of more than 5 m with the system pressure drop about 41.31 kPa when the system volume flow rate is 400 mL/min.
(b) The system has a cooling capability of 240 W when the base temperature is below 80 °C.
(b) When the base temperature is 77.3 °C and the heat source power is 240 W (corresponding to a heat flux of 30 W/cm$^2$), the volume flow rate can be controlled as low as 300 mL/min.

**Acknowledgments:** This work was supported by the National Natural Science Foundation of China (No. 51306125) and Shenzhen Research Foundation of Science & Technology (JCYJ 20130329113322731).

**Author Contributions:** Lei Ma performed the research and wrote the paper; Xuxin Zhao, Hongyuan Sun and Qixing Wu designed and analyzed the data; Wei Liu designed and streamlined the text. All authors have read and approved the final manuscript.

**Conflicts of Interest:** The authors declare no conflict of interest.

### Abbreviations

The following abbreviations are used in this manuscript:

| | |
|---|---|
| $h$ | heat transfer coefficient (W/m$^2$· K) |
| $L$ | length of the outer frame (mm) |
| $L_1$ | distance between inlet and outlet (mm) |
| $L_2$ | distance between two outlets (or inlets) (mm)) |
| $L_\mathrm{w}$ | length of the fins (mm) |
| $\Delta p_{sink}$ | pressure drop between inlet and outlet of the heat sink (Pa) |
| $\Delta p_{total}$ | pressure drop in whole system pipes (Pa) |
| $P_w$ | input heating power (W) |
| $q$ | heat flux at the substrate (W/cm$^2$) |
| $Q_v$ | volume flow rate (mL/min) |
| $t$ | time (min) |
| $T$ | temperature (°C) |
| $T_e$ | ambient temperature (°C) |
| $T_l$ | average liquid temperature (°C) |
| $T_{r,\mathrm{in}}$ | temperature at the inlet of the radiator (°C) |
| $T_{r,out}$ | temperature at the outlet of the radiator (°C) |
| $T_{s,\mathrm{in}}$ | temperature at the inlet of the heat sink (°C) |
| $T_{s,\mathrm{out}}$ | temperature at the outlet of the heat sink (°C) |
| $T_\mathrm{w}$ | base temperature (°C) |
| $W$ | width of the outer frame (mm) |
| $W_\mathrm{c}$ | distance between two fins, the width of the channel (mm) |
| $W_\mathrm{w}$ | width of the fins (mm) |

### Greek Symbol

| | |
|---|---|
| $\alpha$ | the arrangement angel between fins and heat sink side (°) |

## References


1. Hu, Y.; Zeng, L.; Minnich, A.J.; Dresselhaus, M.S.; Chen, G. Spectral Mapping of Thermal Conductivity through Nanoscale Ballistic Transport. *Nat. Nanotechnol.* **2015**, *10*, 701–706. [CrossRef] [PubMed]
2. Zeng, L.; Collins, K.C.; Hu, Y.; Luckyanova, M.N.; Maznev, A.A.; Huberman, S.; Chiloyan, V.; Zhou, J.; Huang, X.; Nelson, K.A.; Chen, G. Measuring phonon mean free path distributions by probing quasiballistic phonon transport in grating nanostructures. *Sci. Rep.* **2015**, *5*. [CrossRef] [PubMed]
3. Zeng, L.; Chen, G. Disparate quasiballistic heat conduction regimes from periodic heat sources on a substrate. *J. Appl. Phys.* **2014**, *116*, 064307. [CrossRef]
4. Zeng, L.; Chiloyan, V.; Huberman, S.; Maznev, A.A.; Peraud, J.-P.M.; Hadjiconstantinou, N.G.; Nelson, K.A.; Chen, G. Monte Carlo study of non-diffusive relaxation of a transient thermal grating in thin membranes. *Appl. Phys. Lett.* **2016**, *108*, 063107. [CrossRef]
5. Chiloyan, V.; Zeng, L.; Huberman, S.; Maznev, A.A.; Nelson, K.A.; Chen, G. A variational approach to extracting the phonon mean free path distribution from the spectral Boltzmann transport equation. **2015**, arXiv:1511.08989. [CrossRef]
6. Tuckerman, D.B.; Pease, R. High-performance heat sinking for VLSI. *IEEE Electron Device Lett.* **1981**, *2*, 126–129. [CrossRef]
7. Vafai, K.; Zhu, L. Analysis of two-layered micro-channel heat sink concept in electronic cooling. *Int. J. Heat Mass Transf.* **1999**, *42*, 2287–2297. [CrossRef]
8. Colgan, E.G.; Furman, B.; Gaynes, M.; Graham, W.S.; LaBianca, N.C.; Magerlein, J.H.; Polastre, R.J.; Rothwell, M.B.; Bezama, R.; Choudhary, R. A practical implementation of silicon microchannel coolers for high power chips. *IEEE Trans. Compon. Packag. Technol.* **2007**, *30*, 218–225. [CrossRef]
9. Peng, X.; Peterson, G. Convective heat transfer and flow friction for water flow in microchannel structures. *Int. J. Heat Mass Transf.* **1996**, *39*, 2599–2608. [CrossRef]
10. Kandlikar, S.G.; Grande, W.J. Evaluation of single phase flow in microchannels for high heat flux chip cooling—Thermohydraulic performance enhancement and fabrication technology. *Heat Transf. Eng.* **2004**, *25*, 5–16. [CrossRef]
11. Steinke, M.E.; Kandlikar, S.G. Single-phase heat transfer enhancement techniques in microchannel and minichannel flows. In Proceedings of the Second International Conference on Microchannels and Minichannels, Rochester, NY, USA, 17–19 June 2004; pp. 17–19.
12. Steinke, M.E.; Kandlikar, S.G. Single-phase liquid friction factors in microchannels. *Int. J. Therm. Sci.* **2006**, *45*, 1073–1083. [CrossRef]
13. Li, J.; Peterson, G.P.; Cheng, P. Three-dimensional analysis of heat transfer in a micro-heat sink with single phase flow. *Int. J. Heat Mass Transf.* **2004**, *47*, 4215–4231. [CrossRef]
14. Sung, M.K.; Mudawar, I. Experimental and numerical investigation of single-phase heat transfer using a hybrid jet-impingement/micro-channel cooling scheme. *Int. J. Heat Mass Transf.* **2006**, *49*, 682–694. [CrossRef]
15. Liu, C.; Teng, J.-T.; Chu, J.-C.; Chiu, Y.-L.; Huang, S.; Jin, S.; Dang, T.; Greif, R.; Pan, H.-H. Experimental investigations on liquid flow and heat transfer in rectangular microchannel with longitudinal vortex generators. *Int. J. Heat Mass Transf.* **2011**, *54*, 3069–3080. [CrossRef]
16. Bower, C.; Ortega, A.; Skandakumaran, P.; Vaidyanathan, R.; Phillips, T. Heat transfer in water-cooled silicon carbide milli-channel heat sinks for high power electronic applications. *Trans. ASME C J. Heat Transf.* **2005**, *127*, 59–65. [CrossRef]
17. Lee, P.-S.; Garimella, S.V.; Liu, D. Investigation of heat transfer in rectangular microchannels. *Int. J. Heat Mass Transf.* **2005**, *48*, 1688–1704. [CrossRef]
18. Qu, W.; Mudawar, I. Experimental and numerical study of pressure drop and heat transfer in a single-phase micro-channel heat sink. *Int. J. Heat Mass Transf.* **2002**, *45*, 2549–2565. [CrossRef]
19. Qu, W.; Mudawar, I. Analysis of three-dimensional heat transfer in micro-channel heat sinks. *Int. J. Heat Mass Transf.* **2002**, *45*, 3973–3985. [CrossRef]
20. Morini, G.L. Single-phase convective heat transfer in microchannels: A review of experimental results. *Int. J. Therm. Sci.* **2004**, *43*, 631–651. [CrossRef]
21. Hawkins-Reynolds, E.; Le, H.; Stephan, R. Development, fabrication, and testing of a liquid/liquid microchannel heat exchanger for constellation spacecrafts. In Proceedings of the International Conference on Environmental Systems, Barcelona, Spain, 11–15 July 2010.

22. Birur, G.C.; Sur, T.W.; Paris, A.D.; Shakkottai, P.; Green, A.A.; Haapanen, S.I. Micro/nano spacecraft thermal control using a MEMS-based pumped liquid cooling system. In Proceedings of the International Society for Optical Engineering (SPIE) International Symposium on Micromachining and Microfabrication, San Francisco, CA, USA, 22–25 October 2001; pp. 196–206.
23. Paris, A.D.; Birur, G.C.; Green, A.A. Development of MEMS microchannel heat sinks for micro/nano spacecraft thermal control. In Proceedings of the ASME 2002 International Mechanical Engineering Congress and Exposition Microelectromechanical Systems, New Orleans, LA, USA, 17–22 November 2002.
24. Bintoro, J.S.; Akbarzadeh, A.; Mochizuki, M. A closed-loop electronics cooling by implementing single phase impinging jet and mini channels heat exchanger. *Appl. Therm. Eng.* **2005**, *25*, 2740–2753. [CrossRef]
25. Chein, R.; Chen, J. Numerical study of the inlet/outlet arrangement effect on microchannel heat sink performance. *Int. J. Therm. Sci.* **2009**, *48*, 1627–1638. [CrossRef]
26. Kraus, A.D.; Aziz, A.; Welty, J. *Extended Surface Heat Transfer*; Wiley: Hoboken, NJ, USA, 2002.
27. Wheeler, A.J.; Ganji, A.R. *Introduction to Engineering Experimentation*, 2nd ed.; Pearson Prentice Hall: Upper Saddle River, NJ, USA, 2004.
28. Sohel, M.R.; Khaleduzzaman, S.S.; Saidur, R.; Hepbasli, A.; Sabri, M.F.M.; Mahbubul, I.M. An experiment investigation of heat transfer enhancement of a minichannel heat sink using $Al_2O_3$-$H_2O$ nanofluid. *Int. J. Heat Mass Transf.* **2014**, *74*, 164–172. [CrossRef]
29. Tullius, J.F.; Bayazitoglu, Y. Effect of $Al_2O_3/H_2O$ nanofluid on MWNT circular fin structures in a minichannel. *Int. J. Heat Mass Transf.* **2013**, *60*, 523–530. [CrossRef]

© 2016 by the authors; licensee MDPI, Basel, Switzerland. This article is an open access article distributed under the terms and conditions of the Creative Commons Attribution (CC-BY) license (http://creativecommons.org/licenses/by/4.0/).